Theoretical Modeling of ISO Results on Planetary Nebula NGC 7027

THE ASTROPHYSICAL JOURNAL, 515:640–648, 1999 April 10

THEORETICAL MODELING OF *ISO* RESULTS ON PLANETARY NEBULA NGC 7027

M. YAN[1] AND S. R. FEDERMAN[2]
Department of Physics and Astronomy, University of Toledo, Toledo, OH 43606
A. DALGARNO[3]
Harvard-Smithsonian Center for Astrophysics, Cambridge, MA 02138
AND
J. E. BJORKMAN[4]
Department of Physics and Astronomy, University of Toledo, Toledo, OH 43606
Received 1998 June 24; accepted 1998 December 1

ABSTRACT

We present a thermal and chemical model of the neutral envelope of planetary nebula NGC 7027. In our model, the neutral envelope is composed of a thin dense shell of constant density and an outer stellar wind region with the usual inverse-square law density profile. The thermal and chemical structure is calculated with the assumption that the incident radiation field on the inner surface equals 0.5×10^5 times Draine's fit to the average interstellar far-ultraviolet field. The rate coefficient for H_2 formation on grains is assumed to be $\frac{1}{5}$ the usual value to take into account the lower dust-gas mass ratio in the neutral envelope of NGC 7027. The calculated temperature in the dense shell decreases from 3000 to under 200 K. Once the temperature drops to 200 K, we assume that it remains at 200 K until the outer edge of the dense shell is reached, so that the observed intensities of CO $J = 16$–15, 15–14, and 14–13 lines can be reproduced. The 200 K temperature can be interpreted as the average temperature of the shocked gas just behind the forward shock front in the framework of the interacting stellar wind theory. We calculate the intensities of the molecular far-infrared rotational lines by using a revised version of the escape probability formalism. The theoretical intensities for rotational lines of CO (from $J = 29$–28 to $J = 14$–13), CH^+, OH, and CH are shown to be in good agreement with *ISO* observations. The H_2 rovibrational line intensities are also calculated and are in agreement with available observations.

Subject headings: infrared: ISM: lines and bands — ISM: molecules — molecular processes — planetary nebulae: individual (NGC 7027)

1. INTRODUCTION

Planetary nebula NGC 7027 has been studied extensively at optical, infrared, submillimeter, millimeter, and radio wavelengths (Middlemass 1990; Hoare, Roche, & Clegg 1992; Graham et al 1993; Volk & Kwok 1997). Its very bright and rich optical spectrum originates from the ionized nebula and is well characterized by the semiempirical photoionization model of Middlemass (1990). The ionized nebula is surrounded by an expanding molecular envelope, which was first discovered by Mufson, Lyon, & Marionni (1975) through detection of CO rotational lines in the millimeter waveband. Photometric studies reveal that NGC 7027 has a large midinfrared excess and a large submillimeter excess that can be attributed to hot and cold grains, respectively (Hoare et al. 1992). The launch of the *Infrared Space Observatory* (*ISO*) made it possible to do far-infrared spectroscopic studies of planetary nebulae. Extensive observations on NGC 7027 with *ISO* showed that NGC 7027 is also very rich in far-infrared emission lines. Liu et al. (1996, 1997) and Cernicharo et al. (1997) reported detections of the pure rotational lines of CO from $J = 14$–13 up to $J = 29$–28, three of CH, five CH^+ lines, and five for OH, and they report the possible detection of one H_2O line. Although the observational characteristics of the ionized region of NGC 7027 are explained by the photoionization model in the framework of the interacting stellar wind theory (Kwok, Purton, & FitzGerald 1978; Kwok 1994), those of the molecular envelope are not. Recently, Volk & Kwok (1997) presented a model of the neutral envelope of NGC 7027 based on *ISO* results of CO $J = 14$–13, 15–14, 16–15, and ortho-H_2O 179.5 μm lines, as well as previous radio and infrared observations. Although their model can account for *ISO* results available to them, it fails to explain the vast amount of other molecular lines now detected by *ISO*. In this paper, we present a thermal-chemical model that is consistent with currently available *ISO* results on NGC 7027 as well as previous results in other wave bands—in particular, the observations for a number of prominent H_2 infrared lines (Treffer et al. 1976; Beckwith et al. 1980; Graham et al. 1993). In addition, we make predictions for the intensities of other H_2 infrared emission lines that may be detectable.

2. THE THERMAL AND CHEMICAL STRUCTURE OF THE NEUTRAL ENVELOPE

Molecular rovibrational lines and atomic fine structure lines are good diagnostics of dense warm neutral clouds (Tielens & Hollenbach 1985; Hollenbach & McKee 1989). For NGC 7027, H_2 rovibrational lines were detected by Treffer et al. (1976) and Beckwith et al. (1980). Subsequently O I 63 μm and C II 157 μm lines (Ellis & Werner 1984) were also seen. The H_2 1–0 S(1) line emission was mapped by Gatley, Depoy, & Fowler (1988) and Graham et al. (1993). Although originally thought to be due to shock excitation (Beckwith et al. 1980), these infrared lines can be interpreted as originating from a dense photodissociation region (Burton, Hollenbach, & Tielens 1990; Graham et al. 1993;

[1] Email: myan@astro1.panet.utoledo.edu.
[2] Email: sfederm@uoft02.utoledo.edu.
[3] Email: adalgarno@cfa.harvard.edu.
[4] Email: jon@physics.utoledo.edu.

Liu et al. 1996). Since the neutral envelope surrounds the ionized nebula, it is subjected to the far-ultraviolet photons from the nebula. It is also influenced by a forward shock in the framework of the largely successful interacting stellar wind theory (Kwok 1994; Volk & Kwok 1997). Thus we construct a model for the neutral envelope in which both photodissociation and a shock play important roles.

The shape of the neutral envelope of NGC 7027 on the sky is largely rectangular (Graham et al. 1993). To simplify our treatment, we use the spherical approximation; the geometry of our model is the same as that of Volk & Kwok (1997). In our model NGC 7027 has a three-component structure: a central ionized region; a thin, neutral, high-density shell of constant density; and a stellar wind region with the usual inverse-square density profile. We assume that the radiation field incident upon the neutral envelope is represented by a $\chi = 0.5 \times 10^5$ Draine field (Draine 1978; Burton et al. 1990; Liu et al. 1996). The density and thickness of the high-density shell are taken to be $n_{\rm H} = 2 \times 10^6$ cm^{-3} and 3×10^{15} cm, respectively. The density at the inner edge of the stellar wind region is taken to be 10^5 cm^{-3}. According to the interacting stellar wind theory, both the high-density shell and the outer stellar wind belong to the same asymptotic giant branch wind (Kwok 1994; Volk & Kwok 1997). Thus the elemental abundances for the dense shell should be the same as those of the stellar wind region, and they are taken to be the standard interstellar medium (ISM) values (Tielens & Hollenbach 1985), since the carbon abundance in the stellar wind region may be much smaller than that of the ionized region (Middlemass 1990) and close to the standard ISM value (Jaminet et al. 1991). The adopted parameters are similar to those of Burton et al. (1990), Liu et al. (1996), and Volk & Kwok (1997).

We adopted the chemical reaction network and rate coefficients from the compilation of Millar, Farquhar, & Willacy (1997) except the photoprocesses, which were taken from the compilation of Sternberg & Dalgarno (1995). We included H, He, C, N, O, Si, S, Cl, and Fe in our model. Except for H_3O^+ and CH_3^+, only three-constituent and smaller species in the Millar et al. (1997) compilation were involved. In all, 1389 reactions and 134 species are considered. We used the H_2 self-shielding formula of Federman, Glassgold, & Kwan (1979). The CO self-shielding and mutual-shielding formula was taken from van Dishoeck & Black (1988); for the high-density shell, the shielding effect was reduced by a factor of about 2.3 (Federman & Yan 1998), since the CO excitation temperature there is much higher than the 10 K adopted by van Dishoeck & Black (1988). Comprehensive studies of CO self-shielding and mutual-shielding in warm, dense clouds are needed for a more detailed study of NGC 7027. They may also be needed for studies of other warm, dense, shocked regions and photodissociation regions. We computed the depth-dependent fractional abundances of chemical species by solving equilibrium chemical equations of the form

$$\sum_{jl} n_{\rm H} k_{ijl}(T) x_j x_l + \sum_j (\Gamma_{ij} + \zeta_{ij}) x_j = x_i \left\{ \sum_{jl} n_{\rm H} k_{jil} x_l + \sum_j [\Gamma_{ji}(z) + \zeta_{ji}] \right\}, \quad (1)$$

where $x_i = n_i/n_{\rm H}$ is the abundance of atom or molecule i, $k_{ijl}(T)$ are the (temperature-dependent) rate coefficients (cm^3 s^{-1}) for chemical reactions between species j and l that lead to the production of i, and $\Gamma_{ij}(z)$ and ζ_{ij} are the photon and cosmic-ray destruction rates (s^{-1}) of species j with products i.

Since rovibrationally excited H_2 plays an important role in the thermal and chemical processes (Tielens & Hollenbach 1985; Sternberg & Dalgarno 1989), we solved the fractional abundance of each H_2 rovibrational level through statistical equilibrium equations as follows:

$$\begin{aligned} x_{vj} \Bigg\{ \sum_{v'j'} [A(vj \rightarrow v'j') + \sum_i n_i Q_i(T; vj \rightarrow v'j')] \\ + \sum_{v^*j^*} P(vj \rightarrow v^*j^*) + \zeta + \sum_i k_{ivj}(T) n_i \Bigg\} \\ = \sum_{v'j'} x_{v'j'} \Bigg[A(v'j' \rightarrow vj) + \sum_i n_i Q_i(T; v'j' \rightarrow vj) \\ + \sum_{v^*j^*} P(v'j' \rightarrow v^*j^*) b(v^*j^* \rightarrow vj) \Bigg] \\ + R\beta(vj) n_{\rm H} x_1 + \sum_{il} k_{ilvj}(T) n_{\rm H} x_i x_l \,. \end{aligned} \quad (2)$$

In these equations $A(vj \rightarrow v'j')$ are quadrupole radiative transition probabilities from levels vj to levels $v'j'$, and $P(vj \rightarrow v^*j^*)$ are the UV excitation rates out of level vj of the ground electronic state to level v^*j^* of an excited electronic state. The parameters $b(v^*j^* \rightarrow vj)$ are the branching ratios of the transitions between levels v^*j^* and vj of the excited and ground electronic states. We followed the approach of Sternberg & Dalgarno (1989) in calculating $P(vj \rightarrow v^*j^*)$ and $b(v^*j^* \rightarrow vj)$; ζ is the cosmic-ray destruction rate. The Q_i are the temperature-dependent rate coefficients for collisions with particles of density n_i that induce transitions from vj to $v'j'$. We use values of Q_i for collisions with H, H_2, He, and electrons from Sternberg & Dalgarno (1989) and Tine et al. (1997). The value R is the rate coefficient for H_2 formation on grains; we adopt a value of 6×10^{-18} cm^3 s^{-1}, since the dust-gas mass ratio in the neutral envelope of NGC 7027 is about 20% the standard value for the ISM (Hoare et al. 1992). The value x_1 is the atomic hydrogen fractional abundance, and $\beta(vj)$ are the fractions of molecules populating levels vj in the process of H_2 formation on grains. We adopt the formula for $\beta(vj)$ given by Sternberg & Dalgarno (1989). The values $k_{ivj}(T)$ are the rate coefficients for chemical reactions between species i and H_2 in level vj that lead to the destruction of H_2; $k_{ilvj}(T)$ are the rate coefficients for chemical reactions between species i and l that lead to the formation of H_2 in level vj. We followed the approach of Sternberg & Dalgarno (1995) when calculating $k_{ivj}(T)$ and $k_{ilvj}(T)$, except that we replaced the H_2 vibrational levels they used by H_2 rovibrational levels.

The relative roles of different chemical processes depend on the gas temperature. The depth-dependent gas temperature was calculated under the assumption of thermal equilibrium:

$$G(T) - L(T) = 0 \,, \quad (3)$$

where $G(T)$ and $L(T)$ are the total heating and cooling rates. The major thermal processes considered by us are grain photoelectric heating, heating from collisional quenching of H_2^*, gas-grain collisional heating (or cooling), cooling through atomic and ionic metastable and fine-structure emission, and molecular rovibrational emission. Our

heating and cooling rate formulas are taken from Sternberg & Dalgarno (1995) and Yan (1996). We adopted a turbulence velocity of 2 km s^{-1} (Jaminet et al. 1991) for the line width in calculating the cooling rates.

Gas-grain collisions are an important cooling channel for dense, warm gases (Hollenbach & McKee 1989). The dust temperature is needed in calculating the rate of this cooling process. It was calculated from the thermal balance between dust absorption and dust emission. We used a formula given in Sternberg & Dalgarno (1989) to calculate the dust temperature except that we assume a minimum dust temperature of 20 K to account for the dust absorption of infrared emission (Tielens & Hollenbach 1985).

We assumed the minimum temperature in the high-density shell to be 200 K, which occurs at the outer boundary. The temperature was needed for fitting of the observed CO $J = 14$–13, 15–14, and 16–15 lines and can be interpreted as due to the heating by the forward shock, which is produced by the two interacting stellar winds (Kwok 1994).

The thermal and chemical structure of the neutral envelope was solved by integrating

$$\frac{dN_i(z)}{dz} = n_{\rm H}\, x_i(z) \tag{4}$$

through a Bulirsch-Stoer adaptive step size integrator (Press et al. 1992), where $x_i(z)$ and $N_i(z)$ are the fractional abundance and column density for species i. The $x_i(z)$ was derived by solving equations (1), (2), and (3) together. Numerically, this was done through the following procedure. First, we solved equations (1) and (2) for fractional abundances using the temperature from the previous step (or an assumed temperature for the first step). Second, we solved equation (3) for the temperature using the derived fractional abundances. We then iterated the two processes until the temperature and fractional abundances converge.

The major results of our calculation are illustrated in Figures 1–3. We note that the photodissociation and photoionization of atomic and molecular species by the diffuse interstellar UV radiation field (from outside the system) are not considered in the model. The H_2 photodissociation rate ξ, which is derived by summing up the products of the UV pumping rates (Sternberg & Dalgarno 1989) and the corresponding dissociation fractions (Stephens & Dalgarno 1972) and the kinetic temperature T, are presented as functions of the radial distance in Figure 1. Within the high-density shell, ξ decreases monotonically from about 10^{-6} s^{-1} at the inner surface to about 10^{-15} s^{-1} at the outer edge, while T also decreases from about 3000 to 200 K. In the stellar wind region, ξ continues to decrease and becomes far less than the cosmic-ray ionization rate at a radial distance of 4×10^{17} cm, the end point of our calculation. The kinetic temperature T starts from a value of about 60 K, after a sharp drop from 200 K at the outer edge of the high-density shell, and decreases monotonically to about 10 K at the end point. Figure 2 shows fractional abundances of

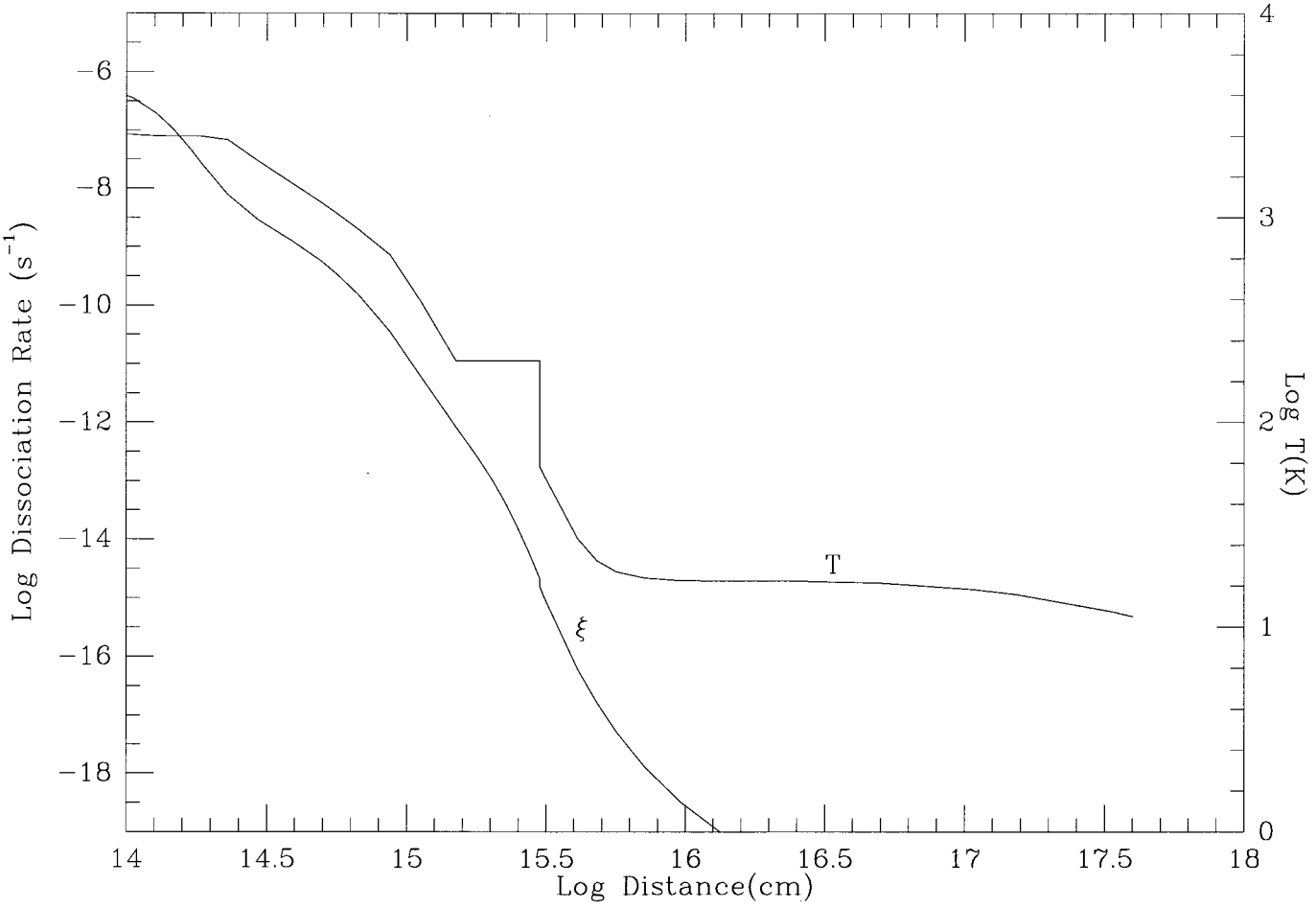

FIG. 1.—H_2 dissociation rate and kinetic temperature as functions of the radial distance from the inner surface of the high-density shell. The high-density shell is on the left, before the sharp jump at 3×10^{15} cm in temperature; the stellar wind region is on the right, after the jump.

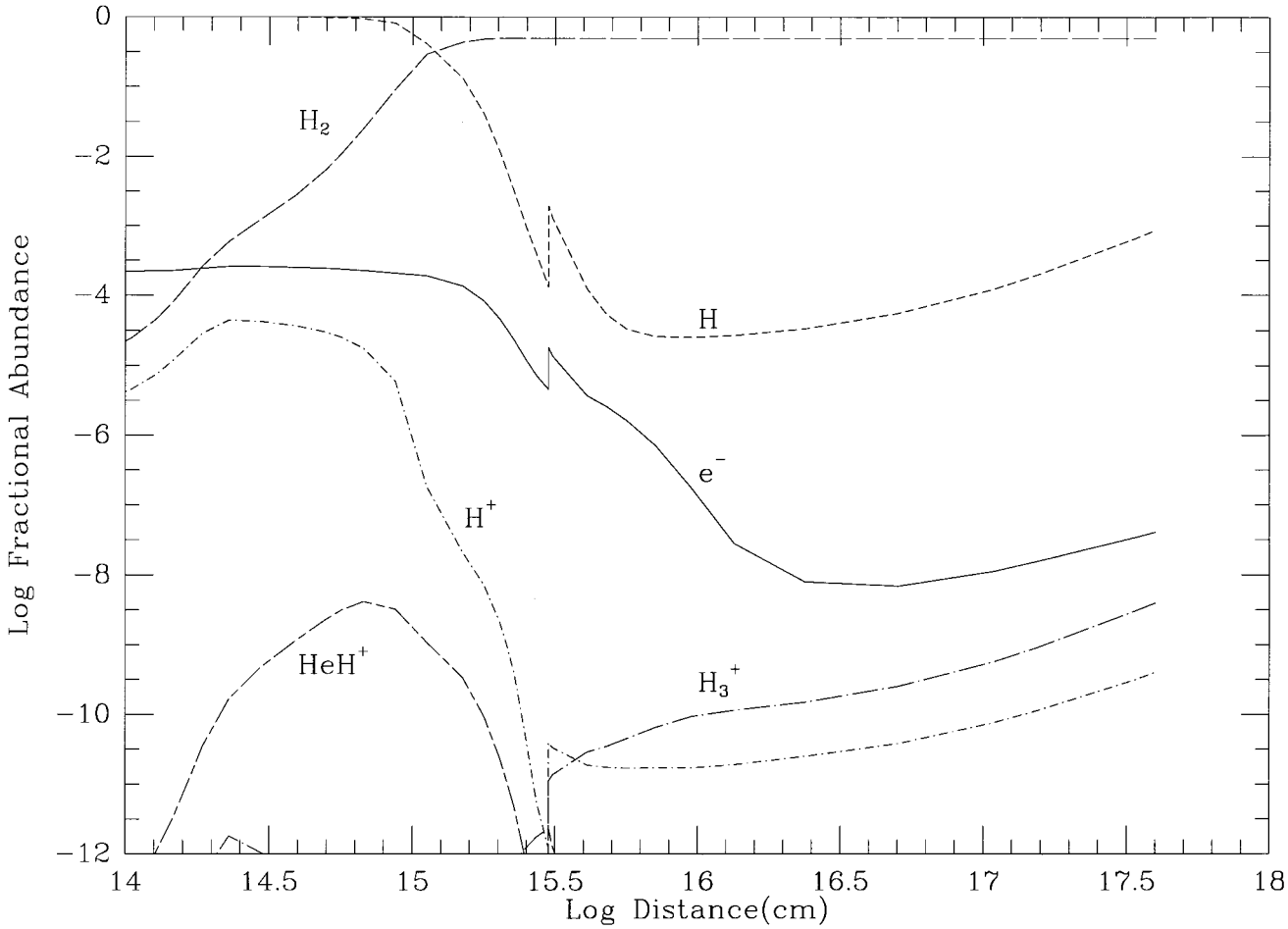

FIG. 2.—Fractional abundances of e, H, H_2, H^+, H_3^+, and HeH^+ as functions of the radial distance from the inner surface of the high-density shell. The high-density shell is on the left, before the sharp jumps at 3×10^{15} cm in fractional abundances of H, H_3^+, and so on; the stellar wind region is on the right, after the jumps.

H, H_2, H^+, H_3^+, HeH^+, and electrons. The fractional abundances of H^+, H_3^+, and HeH^+ are always very small and of negligible observational consequence. Within the high-density shell, the gas is atomic in the inner shell and molecular at the outer boundary. The H_2 abundance increases monotonically from about 10^{-5} to 0.5. The H and electron abundances are nearly constant at 1 and 2×10^{-4} for the inner half shell, but they decrease monotonically to 10^{-4} and 3×10^{-6} at the outer edge. In the stellar wind region, the H_2 and H abundances are almost constant at 0.5 and 10^{-4}, while the electron abundance decreases from about 10^{-5} to about 10^{-8} before it starts to increase and reaches a value of 5×10^{-8} at the end point of our calculation. The increase in H abundance at large radial distances is due to the increase of ζ/n_H, where $\zeta = 1.3 \times 10^{-17}$ s^{-1} is the cosmic-ray ionization rate and the density n_H goes with the inverse square of the radial distance. In Figure 3 we present the fractional abundances of C, O, C^+, CO, OH, CH, H_2O, and CH^+ as functions of radial distance. We concentrate on CO, OH, CH, H_2O, and CH^+, since these species were detected by *ISO* and they exist only in the neutral envelope. In the high-density shell the fractional abundances of OH, CH^+, and H_2O reach their peak values of 10^{-6}, 3×10^{-8}, and 3×10^{-8}, respectively, at about the place where the temperature is about 1000 K. The CH abundance peaks farther outside at a value of 2×10^{-7}, whereas that of CO peaks at the outer edge with almost all carbon locked up in CO. In the stellar wind region, CO contains almost all the carbon. The carbon and oxygen that are not in CO exist almost entirely in atomic form. The abundances of CH, OH, and H_2O increase outward, but the densities of these species are small, since the total density goes with the inverse square of the radial distance.

Since the density and temperature of the stellar wind region are low, the detected *ISO* lines and H_2 infrared lines are predominantly produced in the high-density shell. Thus we only discuss the distribution and major formation and destruction processes for the observed species in the high-density shell. OH and CH^+ exist in regions where the temperature is around 1000 K or higher. OH is produced by the endothermic reaction

$$O + H_2 \rightarrow OH + H \quad (5)$$

and is removed by

$$OH + h\nu \rightarrow O + H\,, \quad (6)$$

$$OH + H \rightarrow O + H_2\,, \quad (7)$$

$$C^+ + OH \rightarrow CO + H^+\,, \quad (8)$$

$$C^+ + OH \rightarrow CO^+ + H\,. \quad (9)$$

The endothermic reaction

$$C^+ + H_2 \rightarrow CH^+ + H \quad (10)$$

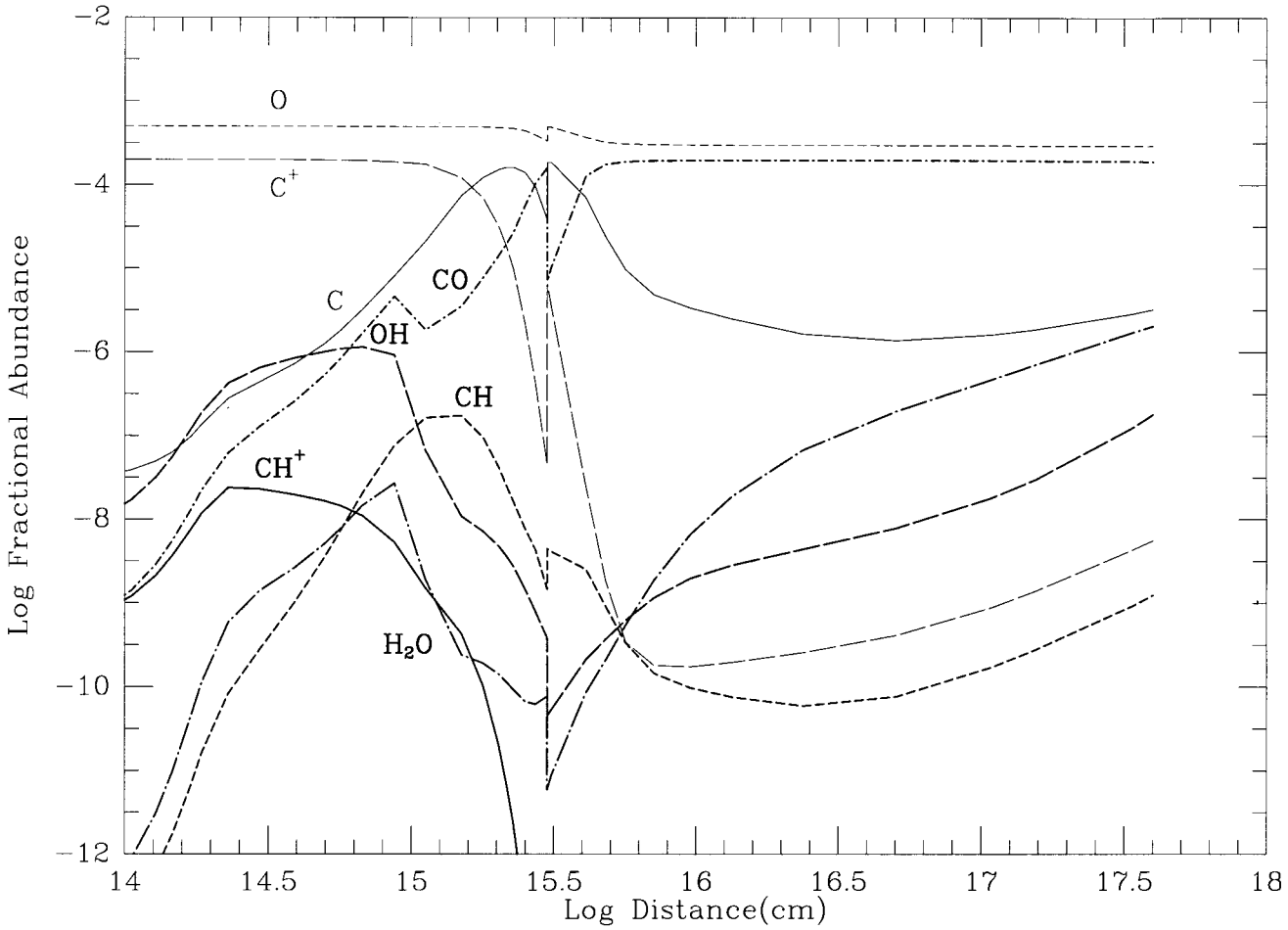

FIG. 3.—Fractional abundances of C, O, C^+, CO, OH, CH, H_2O, and CH^+ as functions of the radial distance from the inner surface of the high-density shell. The high-density shell is on the left, before the sharp jumps at 3×10^{15} cm in fractional abundances of OH, CH, CO, and so on; the stellar wind region is on the right, after the jumps.

leads to CH^+, and CH^+ is removed by

$$CH^+ + H \rightarrow C^+ + H_2 , \quad (11)$$

$$CH^+ + h\nu \rightarrow C + H^+ , \quad (12)$$

$$CH^+ + e^- \rightarrow C + H . \quad (13)$$

The molecule CO is abundant in the outer boundary layer of the high-density shell. At the outer edge of this layer where the temperature is 200 K, almost all carbon is locked up in CO. At the inner part of this layer where the temperature ranges from 200 to about 1000 K, the CO abundance is smaller. This warm high-density boundary layer is the region where high-J CO rotational lines originate. In the region, CO is formed through reaction (8) and through reaction (9) followed by

$$CO^+ + H \rightarrow CO + H^+ , \quad (14)$$

and removed through

$$CO + h\nu \rightarrow C + O . \quad (15)$$

The boundary layer of the high-density shell is also where CH resides. In the inner region of the boundary, where the temperature ranges from several 100 K to about 1000 K, CH is produced by

$$CH^+ + H_2 \rightarrow CH_2^+ + H , \quad (16)$$

$$CH_2^+ + H_2 \rightarrow CH_3^+ + H , \quad (17)$$

$$CH_2^+ + e^- \rightarrow CH + H , \quad (18)$$

$$CH_3^+ + e^- \rightarrow CH + H_2 . \quad (19)$$

At the edge of the high-density shell where the temperature is 200 K, CH is produced by

$$C + H_2 \rightarrow CH_2 + h\nu , \quad (20)$$

$$H + CH_2 \rightarrow CH + H_2 . \quad (21)$$

CH is always removed by

$$CH + H \rightarrow C + H_2 , \quad (22)$$

$$CH + h\nu \rightarrow C + H , \quad (23)$$

$$CH + h\nu \rightarrow CH^+ + e^- . \quad (24)$$

We also made a calculation including the influence of the diffuse interstellar radiation field. The thermal, chemical, and ionizational structures of the high-density shell are unaltered. Those of the outer stellar wind region show a modest change, but the corresponding temperature and

abundances are still too small to have observational consequences on *ISO* data and H_2 infrared data.

3. EMISSION-LINE INTENSITIES

We computed the intensities of CO, OH, CH, and CH^+ rotational lines based on the fractional abundances presented in the last section. Far-infrared emission from the low-density stellar wind region is negligible, because the temperature and density of the region are too low. Thus only the high-density shell was included in our calculation. We employed a modified escape probability formalism. For each molecular species, we first assumed all emission lines to be optically thin, and we calculated the fractional population of rotational levels at each depth step by solving the statistical equilibrium equations (Yan & Dalgarno 1997). Then we computed the opacity and escape probability (de Jong, Dalgarno, & Boland 1980) of each rotational line traversing the whole depth of the high-density shell. At this point, the fractional abundances of rotational levels at each depth step were recomputed by solving the statistical equilibrium equations where now Einstein A values were replaced by the effective A values, which are products of the A values and the corresponding escape probabilities. We iterated the above procedure until the fractional abundances of rotational levels converged. The intensity of each rotational line was computed by integrating the effective emissivity through the whole depth of the high-density shell. The effect of stimulated absorption and emission from dust-emitted infrared continuum radiation is included in our calculation.

In solving the statistical equilibrium equations for molecular rotational levels, Einstein A values and collisional excitation rate coefficients were needed. Molecular lines in the high-density shell are excited by collisions with H and H_2. Electron impact excitation is negligible, since the fractional abundance of electrons is very small. For CO, we included the lowest 40 rotational levels of the ground vibrational level in our calculation. We adopted the energy levels, Einstein A values, and H_2 impact rate coefficients of McKee et al. (1982) and H impact rate coefficients of Chu & Dalgarno (1975). For OH, we included the lowest 10 rotational levels. The energy levels and Einstein A values were taken from Offer & van Dishoeck (1992) and Destombes et al. (1977), respectively. When the temperature is high, the H_2 impact quenching rate coefficients are not sensitive to the temperature (Dewangan, Flower, & Alexander 1987; Offer & van Dishoeck 1992). We assumed that they are independent of the temperature, and we used the high-temperature (600 K) H_2 impact-quenching rate coefficients of Offer & van Dishoeck (1992). The excitation rate coefficients were calculated from detailed balance. There are not any available theoretical or experimental data on the H impact rate coefficients. The H impact rate coefficients are typically within 1–10 times the corresponding H_2 impact values, and we assumed them to be the same as the corresponding H_2 impact values to fit the observed OH line fluxes. For CH, we also included the lowest 10 rotational levels. The energy levels and Einstein A values were taken from Brown & Evenson (1983). There are no data available on the H and H_2 impact rate coefficients for CH. We assumed that they are the same and equal to 1.3 times the corresponding H_2-OH impact rate coefficients to fit the observations. For CH^+, we included the lowest 20 rotational levels. Neither theoretical nor experimental data are available on the H and H_2 impact rate coefficients. We assumed the H and H_2 impact rate coefficients to be the same. To fit observations, we chose H_2 collisional quenching rate coefficients that are 2.5 times the corresponding HCO^+ values (Turner 1994). The upward rate coefficients were derived from detailed balance. The molecular line width was needed in calculating the opacities and the effective A values; we adopted a value of 2 km s^{-1} (Jaminet et al. 1991).

The observed and computed intensities for CO, OH, CH and CH^+ rotational lines are listed in Tables 1–4. The theoretical CO line fluxes are in very good agreement with the observed fluxes except for $J = 21$–20 up to $J = 24$–23, where the theoretical values are 2–3 times the observed values. The discrepancies for these four CO lines may be attributed to *ISO* calibration or data reduction uncertainty, since the spectra are weak and noisy (Liu et al. 1996). Except for the 119.34 μm line, the calculated OH line fluxes agree with the observed values with the maximum deviation being less than 20% (see Table 2). The 119.34 μm line emis-

TABLE 1

OBSERVED AND COMPUTED CO LINE FLUXES OF NGC 7027

$\lambda_{vac}(\mu m)$	Identification	Flux (Observed)[a]	Flux (Theoretical)[a]
186.00.....	$J = 14$–13	22.5	23.1
173.63.....	$J = 15$–14	21.2	19.7
162.81.....	$J = 16$–15	17.8	15.8
153.27.....	$J = 17$–16	10.0	12.4
144.78.....	$J = 18$–17	9.04[b]	10.0
137.20.....	$J = 19$–18	12.1[b]	8.61
130.37.....	$J = 20$–19	8.44[b]	7.84
124.19.....	$J = 21$–20	4.95[b]	7.44
118.58.....	$J = 22$–21	5.13[b]	7.21
113.46.....	$J = 23$–22	3.03[b]	7.00
108.76.....	$J = 24$–23	4.80[b]	6.75
104.44.....	$J = 25$–24	9.56[b]	6.43
100.46.....	$J = 26$–25	~ 10	6.05
96.77.....	$J = 27$–26	~ 10	5.61
90.16.....	$J = 29$–28	< 10	4.64

[a] In 10^{-20} W cm^{-2}.
[b] Weak and noisy.

TABLE 2

OBSERVED AND COMPUTED OH LINE FLUXES OF NGC 7027

$\lambda_{vac}(\mu m)$	Identification	Flux (Observed)[a]	Flux (Theoretical)[a]
119.34.....	$^2\Pi_{3/2}\, J = \frac{5}{2}-\frac{3}{2}$	15.3 ± 1.1	29.5[b]
84.51	$^2\Pi_{3/2}\, J = \frac{7}{2}-\frac{5}{2}$	19.8 ± 1.5	22.3
65.20	$^2\Pi_{3/2}\, J = \frac{9}{2}-\frac{7}{2}$	< 24 (3 σ)	3.9
163.26.....	$^2\Pi_{1/2}\, J = \frac{3}{2}-\frac{1}{2}$	6.2 ± 0.7	4.9
98.73	$^2\Pi_{1/2}\, J = \frac{5}{2}-\frac{3}{2}$	6.9 ± 1.2	7.0
79.15	$^2\Pi_{1/2-3/2}\, J = \frac{1}{2}-\frac{3}{2}$[c]	17.6 ± 2.3	17.8

[a] In 10^{-20} W cm^{-2}.
[b] The flux may be reduced to about 15 if we include the effect of absorption by interstellar OH.
[c] From $^2\Pi_{1/2}\, J = \frac{1}{2}$ to $^2\Pi_{3/2}\, J = \frac{3}{2}$.

TABLE 3

OBSERVED AND COMPUTED CH LINE FLUXES OF NGC 7027

$\lambda_{vac}(\mu m)$	Identification	Flux (Observed)[a]	Flux (Theoretical)[a]
149.2.....	$^2\Pi_{3/2}(F_2)J = \frac{3}{2}-\frac{1}{2}$	4.2	4.1[b]
115.7.....	$^2\Pi_{3/2}(F_2)J = \frac{5}{2}-\frac{3}{2}$	2.0	1.6
180.6.....	$^2\Pi_{1/2}(F_1)J = \frac{5}{2}-\frac{3}{2}$	3.3	3.9
118.7.....	$^2\Pi_{1/2}(F_1)J = \frac{7}{2}-\frac{5}{2}$	~2.0	1.8

[a] In 10^{-20} W cm^{-2}.

[b] The flux may be reduced to about 2.7 if we include the effect of absorption by interstellar CH.

sion can be absorbed by interstellar OH molecules, since the line ends in the rotational ground state. Indeed, there is an interstellar cloud in the sight line with strong Na absorption lines, and the velocity of the cloud coincides with the central velocity of the approaching high-density half-shell (Dinerstein, Sneden, & Uglum 1995; Jaminet et al. 1991). Interstellar clouds with strong absorption lines typically have OH column densities of about 10^{14} cm^{-2} (van Dishoeck & Black 1986), which corresponds to an opacity of about 2 for the line assuming a velocity width of 4 km s^{-1}. Therefore, up to half of the theoretical 119.34 μm line flux may be absorbed by interstellar OH, and the resultant flux of about 15×10^{-20} W cm^{-2} is in good agreement with the observed value of 15.3×10^{-20} W cm^{-2}. Interstellar absorption of the OH 79.15 μm line that also ends in the rotational ground state may reduce the calculated flux by as much as 20%. After including this effect, the deviation of the theoretical flux from the observed value is still less than 20%. Measurements of OH absorption would yield the column density of interstellar OH and provide additional constraints on our model. The derived CH line fluxes (Table 3) are in good agreement with the observed values. The calculated fluxes change somewhat with the adopted collisional rate coefficients, adding some degree of uncertainty into our result.

Liu et al. (1997) argued against identifying the 149.2 μm line with HeH^+ and favored a CH origin. Our Table 3 seems to support their assertion. However, as in the case of the OH line at 119.34 μm, the CH 149.2 μm line emission in the approaching high-density half-shell may be absorbed by interstellar CH molecules. The typical CH column density of interstellar clouds with strong absorption lines is about 4×10^{13} cm^{-2} (van Dishoeck & Black 1986), which corresponds to an opacity of about 0.5 for this line assuming a velocity width of 4 km s^{-1}. Therefore, about $\frac{1}{3}$ of the observed 149.2 μm line flux may be from HeH^+ at the edge of the ionized nebula (Cecchi-Pestellini & Dalgarno 1993). Future optical measurements of CH absorption are needed to determine the column density of interstellar CH and provide a better constraint on the HeH^+ flux.

The computed CH^+ line fluxes are in excellent agreement with observed values (see Table 4) except for the 179.6 μm line, which also coincides with an ortho-H_2O line. Thus we estimate the water contribution to the 179.6 μm line flux to be 4×10^{-20} W cm^{-2}. Further discussion on the possible H_2O emission is presented in the next section.

We have also used other line widths (1 and 5 km s^{-1}) and other escape probability formulas (Neufeld & Kaufman 1993; Osterbrock 1989) in our calculation. The relative line strengths of the species are essentially the same. We conclude that the theoretical and observational fluxes of CO, OH, CH, and CH^+ lines are in good agreement. The agreement provides strong support for our model.

We computed the H_2 infrared spectrum generally following the approach of Sternberg & Dalgarno (1989), but we also included the effect of formation of H_2 in rovibrationally excited levels through chemical reactions. We included the extinction effect of the grains in the envelope by assuming a $1/\lambda$ extinction law and a visual extinction of 3 (Middlemass 1990). Our results indicate that H_2 is pumped predominantly by ultraviolet fluorescence and formation on grains, but chemical reactions that lead to the formation of H_2 in excited levels can contribute up to 5%. Observational results exist for a number of prominent lines of H_2. The observed and computed fluxes for these lines are listed in Table 5, and they agree quite well. Our calculation is also in good agreement with the result of a recent mapping of NGC 7027 in the H_2 $v = 1$–0 S(1) line by Graham et al. (1993). We derived an intensity of 4.6×10^{-4} ergs s^{-1} cm^{-2} sr^{-1} for the line of sight through the center of the neutral envelope. After subtracting the He I 2.11 μm contribution, the average intensity for the central region from Graham et al. (1993) is 5×10^{-4} ergs s^{-1} cm^{-2} sr^{-1}. We also show predicted fluxes for the 30 strongest H_2 lines in Table 6 and predicted fluxes for the 15 strongest H_2 lines in the K band in Table 7. We note that the predicted fluxes for the H_2 pure rotational lines in Table 6 are rather uncertain (with an accuracy of a factor of a few), since these fluxes depend on the rates of reactions of heavy elements with H_2 in each pure rotational level and reverse reactions that form H_2 in each pure rotational level. Considerable uncertainties exist in the rate coefficients for these reactions and in the elemental abundances. The transitions in Table 7 are mainly those

TABLE 4

OBSERVED AND COMPUTED CH^+ LINE FLUXES OF NGC 7027

$\lambda_{vac}(\mu m)$	Identification	Flux (Observed)[a]	Flux (Theoretical)[a]
179.61.....	$J = 2$–1	15.1 ± 0.5	11.0
119.86.....	$J = 3$–2	21.8 ± 1.7	19.7
90.02.....	$J = 4$–3	23.2 ± 2.5	23.9
72.15.....	$J = 5$–4	25.0 ± 4.1	24.9
60.26.....	$J = 6$–5	24.1 ± 3.3	23.6

[a] In 10^{-20} W cm^{-2}.

TABLE 5

OBSERVED AND COMPUTED H_2 LINE FLUXES OF NGC 7027

Identification	$\lambda_{vac}(\mu m)$	Flux (Observed)[a]	Flux (Theoretical)[a]
$v = 1$–0S(1)	2.122	14 ± 1[b]	13.21
$v = 1$–0Q(1).....	2.407	~10[c]	13.81
$v = 1$–0Q(3).....	2.424	~10[c]	10.05
$v = 1$–0S(2)	2.034	<6[b]	4.18
$v = 1$–0Q(2).....	2.413	<5[c]	4.20
$v = 1$–0S(0)	2.223	4.6 ± 0.7[b]	3.62
$v = 2$–1S(1)	2.248	1 ± 0.5[b]	0.87

[a] In 10^{-20} W cm^{-2}.

[b] From Beckwith et al. 1980.

[c] From Treffers et al. 1976.

TABLE 6

PREDICTED FLUXES OF THE 30 STRONGEST H_2 LINES FROM NGC 7027

Identification	$\lambda_{vac}(\mu m)$	Flux (Theoretical)[a]
$v = 1–0S(7)$	1.748	1.166
$v = 1–0S(5)$	1.836	3.834
$v = 1–0S(4)$	1.892	2.183
$v = 1–0S(3)$	1.958	9.103
$v = 1–0S(2)$	2.034	4.175
$v = 2–1S(3)$	2.074	0.898
$v = 1–0S(1)$	2.122	13.205
$v = 1–0S(0)$	2.223	3.621
$v = 1–0Q(1)$.....	2.407	13.805
$v = 1–0Q(2)$.....	2.413	4.199
$v = 1–0Q(3)$.....	2.424	10.054
$v = 1–0Q(4)$.....	2.437	2.600
$v = 1–0Q(5)$.....	2.455	5.083
$v = 1–0Q(6)$.....	2.476	1.161
$v = 1–0Q(7)$.....	2.500	2.037
$v = 1–0O(2)$.....	2.627	3.901
$v = 1–0O(3)$.....	2.803	12.690
$v = 1–0O(4)$.....	3.004	3.619
$v = 1–0O(5)$.....	3.235	6.546
$v = 1–0O(6)$.....	3.501	1.220
$v = 1–0O(7)$.....	3.808	1.668
$v = 0–0S(8)$	5.053	13.125
$v = 0–0S(7)$	5.511	76.965
$v = 0–0S(6)$	6.109	71.762
$v = 0–0S(5)$	6.909	220.388
$v = 0–0S(4)$	8.026	124.266
$v = 0–0S(3)$	9.665	247.500
$v = 0–0S(2)$	12.279	64.614
$v = 0–0S(1)$	17.035	47.283
$v = 0–0S(0)$	28.221	2.387

[a] in 10^{-20} W cm^{-2}.

observed in the planetary nebula BD $+30°3639$ (Shupe et al. 1998), although there are differences in the relative fluxes.

4. DISCUSSION AND CONCLUSIONS

So far we concentrated on the high-density shell, although we presented the thermal and chemical structure of the stellar wind region as well. Jaminet et al. (1991) mapped NGC 7027 in the $J = 3–2$ and 2–1 lines of CO. They showed that the kinetic temperature is 30 ± 3 K at a radius of 8″ ($r = 1.2 \times 10^{17}$ cm) and varies with radius approximately like $r^{-0.85}$, while the CO:H_2 abundance ratio is $2^{+2}_{-1} \times 10^{-4}$. Figures 1 and 3 show that the computed kinetic temperature and CO:H_2 abundance ratio are largely in agreement with observation. [Note that the distance (D) in these figures is measured from the inner radius of the high-density shell so that $D = (r - 6.8 \times 10^{16})$ cm.] Thus our model supports the assertion of Jaminet et al. (1991) that there is a considerable increase in heavy element abundances, particularly that of carbon (the carbon abundance in the ionized region is much higher than the ISM value), during the last 1000 yr of mass loss from the central star. We also made a calculation of the thermal and chemical structure of the high-density shell by assuming the heavy element abundances to be the same as those of the ionized region. We then computed the CH^+ and CH fluxes based on the model. We must assume unreasonably low collisional excitation rate coefficients to force the calculated fluxes to be in agreement with observations. The logical conclusion is that the heavy element abundances in the neutral envelope are close to the ISM values. Future submillimeter observations of C I 609 μm emission from NGC 7027 may provide further confirmation.

We removed the assumption of a constant temperature of 200 K in the outer boundary layer of the high-density shell to see the effect of the shock. The computed temperature decreased rapidly to less than 20 K toward the outer boundary. The resulting intensities of the CO $J = 14–13$, 15–14, and 16–15 lines fall far short of the observed values, while those of the CO high-J lines such as 27–26 and 26–25 remain unchanged. Our model results suggest, therefore, that the far-infrared emission lines of NGC 7027 originate from the high-density shell, whose inner part is a photodissociation region (PDR) and outer part is a shocked region.

We also varied the thickness of the high-density shell in the range of $(2–4) \times 10^{15}$ cm and the temperature of the shocked region in the range of 100–400 K. The influence on the predicted intensities is negligible for CH^+ and OH and small for CH, because these species are most abundant in the high-temperature (~ 1000 K) PDR. The influence on the CO low-J ($J < 20$) line intensities, however, is significant. About half of the CO low-J line intensities are produced in the shocked region. The higher the temperature of the shocked region, the higher the J at which the observed CO intensity peaks. Agreement with observations is best with a shell thickness of 3×10^{15} cm and a shocked gas temperature of 200 K, which are the adopted values in our model.

A number of water far-infrared lines have been tentatively identified (Cernicharo et al. 1997; Liu et al. 1997). They are ortho-H_2O 179.6, 174.6, 108.05, and 75.39 μm lines with fluxes of (4, 1.5, 5.5, and 6.6) $\times 10^{-20}$ W cm^{-2}, respectively. Our model cannot reproduce these line fluxes. The lines may originate from a thin layer of shocked gas in the high-density shell just inside the stellar wind region where the temperature ranges from about 300 to about 1000 K. Shock models (Draine, Roberge, & Dalgarno 1983) showed that at such temperatures a significant fraction of oxygen exists in H_2O. The required H_2O column density to fit the observation (Volk & Kwok 1997) can be reached in a shell that is a small fraction of the high-density shell. Furthermore, the

TABLE 7

PREDICTED FLUXES OF THE 15 STRONGEST K-BAND H_2 LINES FROM NGC 7027

Identification	$\lambda_{vac}(\mu m)$	Flux (Theoretical)[a]
$v = 1–0S(2)$	2.034	4.175
$v = 3–2S(5)$	2.066	0.152
$v = 2–1S(3)$	2.074	0.898
$v = 1–0S(1)$	2.122	13.205
$v = 3–2S(4)$	2.128	0.072
$v = 2–1S(2)$	2.154	0.372
$v = 3–2S(3)$	2.201	0.212
$v = 1–0S(0)$	2.223	3.621
$v = 2–1S(1)$	2.248	0.866
$v = 3–2S(2)$	2.287	0.085
$v = 4–3S(3)$	2.344	0.070
$v = 2–1S(0)$	2.356	0.248
$v = 3–2S(1)$	2.386	0.165
$v = 1–0Q(1)$.....	2.407	13.805
$v = 1–0Q(2)$.....	2.413	4.199

[a] in 10^{-20} W cm^{-2}.

observed relative strengths of the water lines are similar to the theoretical result for shocked gas (Neufeld & Melnick 1987). Therefore the temperature of 200 K we adopted for the shocked region can be reinterpreted as the average temperature of the shocked region, and water emission can be accounted for, while the results of our calculation remain unaltered. Detailed modeling of the shock resulting from interacting stellar winds, which is beyond the scope of this paper, is needed for a comprehensive study of the H_2O far-infrared emission. If the detection of water lines is confirmed, it further supports our assertion that the neutral envelope of NGC 7027 is under the combined influence of photodissociation and a shock.

The CH^+ emission-line intensities from our model are in good agreement with the observed values. Our model suggests that the high-CH^+ column density (Liu et al. 1997) can be attributed to the high temperature of the CH^+ formation region, which may be an important step in solving the long standing puzzle of the high CH^+ fractional abundance in the general ISM.

Based on our study in this paper, we draw the following conclusions:

1. The neutral envelope of NGC 7027 is under the combined influence of photodissociation and a shock.
2. It is highly likely that the carbon abundance in the neutral envelope is much lower than that in the ionized region.
3. The CH^+, OH and CH lines originate from the dense, high-temperature ($\sim$1000 K) PDR.
4. High-J (from $J = 29$–28 down to $J = 17$–16) CO lines originate from the dense, high-temperature PDR, whereas about half the intensities of low-J (16–15, 15–14, and 14–13) CO lines originate from the dense, high-temperature PDR; the rest come from the outer dense shocked region.

We thank the referee, Sun Kwok, for suggestions that led to significant improvements of this paper. S. R. F. and M. Y. gratefully acknowledge support from NASA grant NAG5-4957 under the LTSA program. A. D. acknowledges support from the National Science Foundation, Division of Astronomy.

REFERENCES

Beckwith, S., et al. 1980, AJ, 85, 886
Brown, J. M., & Evenson, K. M. 1983, ApJ, 268, L51
Burton, M. G., Hollenbach, D. J., & Tielens, A. G. G. M. 1990, ApJ, 365, 620
Cecchi-Pestellini, C., & Dalgarno, A. 1993, ApJ, 413, 611
Cernicharo, J., et al. 1997, ApJ, 483, L65
Chu, S. I., & Dalgarno, A. 1975, Proc. R. Soc. London A, 342, 191
de Jong, T., Dalgarno, A., & Boland, A. 1980, A&A, 91, 68
Destombes, J. L., Marliere, C., Baudry, A., & Brillet, J. 1977, A&A, 60, 55
Dewangan, D. P., Flower, D. R., & Alexander, M. H. 1987, MNRAS, 226, 505
Dinerstein, H. L., Sneden, C., & Uglum, J. 1995, ApJ, 447, 262
Draine, B. T. 1978, ApJS, 36, 595
Draine, B. T., Roberge, W. G., & Dalgarno, A. 1983, ApJ, 264, 485
Ellis, H. B., & Werner, M. W. 1984, BAAS, 16, 462
Federman, S. R., Glassgold, A. E., & Kwan, J. 1979, ApJ, 227, 446
Federman, S. R., & Yan, M. 1998, in preparation
Gatley, I., Depoy, D. L., & Fowler, A. M. 1988, Science, 242, 1264
Graham, J. R., et al. 1993, AJ, 105, 250
Hoare, M. G., Roche, P. F., & Clegg, R. E. S. 1992, MNRAS, 258, 257
Hollenbach, D., & McKee, C. F. 1989, ApJ, 342, 306
Jaminet, P. A., et al. 1991, ApJ, 380, 461
Kwok, S. 1994, PASP, 106, 344
Kwok, S., Purton, C. R., & FitzGerald, M. P. 1978, ApJ, 219, L125
Liu, X.-W., et al. 1996, A&A, 315, L257
———. 1997, MNRAS, 290, L71
McKee, C. F., Storey, J. W., Watson, D. M., & Green, S. 1982, ApJ, 259, 647
Middlemass, D. 1990, MNRAS, 244, 294
Millar, T. J., Farquhar, P. R. A., & Willacy, K. 1997, A&AS, 121, 139
Mufson, S. L., Lyon, J., & Marionni, P. A. 1975, ApJ, 201, L85
Neufeld, D. A., & Kaufman, M. J. 1993, ApJ, 418, 263
Neufeld, D. A., & Melnick, G. J. 1987, ApJ, 322, 266
Offer, A. R., & van Dishoeck, E. F. 1992, MNRAS, 257, 377
Osterbrock, D. E. 1989, Astrophysics of Gaseous Nebulae and Active Galactic Nuclei (Mill Valley: University Science Books)
Press, W. H., Teukolsky, S. A., Vetterling, W. T., & Flannery, B. P. 1992, in Numerical Recipes (Cambridge: Cambridge Univ. Press), 718
Shupe, D. L., et al. 1998, ApJ, 498, 267
Stephens, T. L., & Dalgarno, A. 1972, J. Quant. Spectrosc. Radiat. Transfer, 12, 569
Sternberg, A., & Dalgarno, A. 1989, ApJ, 338, 197
———. 1995, ApJS, 99, 565
Tielens, A. G. G. M., & Hollenbach, D. 1985, ApJ, 291, 722
Tine, S., Lepp, S., Gredel, R., & Dalgarno, A. 1997, ApJ, 481, 282
Treffers, R. R., Fink, V., Larson, H. P., & Gautier, T. N. 1976, ApJ, 209, 793
Turner, B. E. 1994, ApJ, 430, 727
van Dishoeck, E. F., & Black, J. H. 1986, ApJS, 62, 109
———. 1988, ApJ, 334, 771
Volk, K., & Kwok, S. 1997, ApJ, 477, 722
Yan, M. 1996, Ph.D. thesis, Harvard University
Yan, M., & Dalgarno, A. 1997, ApJ, 481, 296